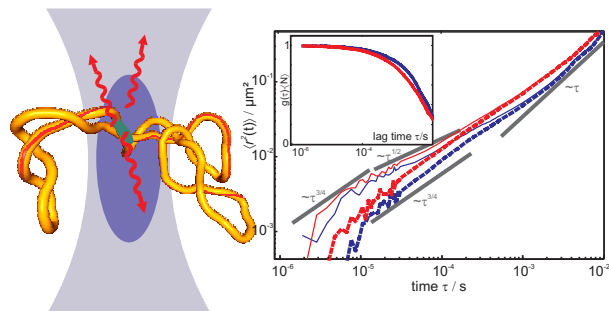# For Contents Page:

Abstract:

Superhelicity accelerates internal dynamics of DNA – Brownian dynamics modeling of fluorescence correlation spectroscopy.

Image:

Dynamics of a fluorophore attached to superhelical DNA: FCS experiments simulated by Brownian dynamics

Tomasz Wocjan[*]   Jan Krieger[*]   Oleg Krichevsky[†]

Jörg Langowski[*‡]

August 20, 2009

Abstract

We investigated the dynamics of a single-fluorophore-labeled pUC18 plasmid through a Brownian dynamics algorithm, followed up by a simulation of the fluorescence correlation spectroscopy (FCS) process. Recent experimental FCS measurements indicated a sensitivity of the monomer mean square displacements in DNA circles towards superhelicity. Simulations with homogeneous DNA elasticity and local straight equilibrium are not sufficient to reproduce this observed behavior. But inserting permanently bent sequences into the DNA, which favor end loop formation, caused a dependence of the calculated FCS correlation curves on superhelical density. Furthermore, our simulations allow us to take into account the orientation of the fluorophore in polarized excitation, which might explain the observed appearance of a Rouse-like regime at intermediate time scales.

[*]Biophysics of Macromolecules, German Cancer Research Center, Im Neuenheimer Feld 280, 69120 Heidelberg, Germany

[†]Physics Department, Ben-Gurion University, Beer-Sheva 84105, Israel

[‡]E-mail: `jl@dkfz-heidelberg.de`

1 Introduction

DNA prokaryote cells, and also in yeast, is circular and in addition often plectone-mically supercoiled, a conformation which resembles a twisted telephone cord (see Figure 1). An important topological invariant in superhelical DNA is the number of times the two DNA strands wind around each other - the linking number Lk. It can be expressed as the sum of two geometrical quantities[1] $Lk = Tw + Wr$. The twist Tw describes the twisting of one strand around the other in a planar conformation, while the writhe Wr is a measure of the extent to which the DNA axis coils and folds in three dimensions. The linking number difference $\Delta Lk = Lk - Lk_0$ quantifies the amount of excess superhelicity introduced into the circular structure with respect to the relaxed B-DNA molecule, which has one right-handed twist per 3.4 nm.

Supercoiling is highly important for biological processes e.g. bringing two specific DNA sites in close contact, which is required for transcription, replication and recombination.[2] A thorough understanding of these processes require quantitative statements about the internal dynamics of single sites on the DNA dependent on the superhelicity. Until recently experimental information on circular DNA was available in form of the translational and rotational diffusion coefficients and the dominant mode of internal fluctuations from dynamical light scattering.[3,4] However, the observation of a precisely defined site on the DNA can give much deeper insight into the internal dynamics of the molecules, which in connection with appropriate models will then enable understanding the biologically important mechanism of site- site interaction in large DNA molecules. To this aim, the single monomer dynamics of fluorophore-labeled super-helical DNA have recently been measured with fluorescence correlation spectroscopy (FCS).[5] FCS[6,7] is a powerful experimental method for measuring the dynamics of molecules. It has been used to measure (anomalous) diffusion,[8,9] flow,[10,11] fast rotational motion,[12,13] photophysical properties[14] and miscellaneous chemical reactions[6] both in vitro and in vivo, i.e. in living cells. FCS is capable of resolving the internal dynamics of labeled molecules that are larger than the focal volume.[15,16] It is based on a correlation analysis of the fluorescence photons emitted by molecules that move in a

tiny laser focus (typical volume of 1 femtolitre) inside the sample.

In the experimental study[5] an acceleration of the dynamics on all time scales was observed with increasing superhelicity. Interestingly on intermediate time scales the monomer dynamics showed characteristics reminiscent of a Rouse model with mean-square displacement $\propto t^{1/2}$. But for a semiflexible polymer such as DNA it is expected that at length scales larger than the persistence length the kinetics should be governed by Zimm dynamics, which is valid for flexible polymers with hydrodynamic interactions. In this work we studied the effect of superhelicity on the dynamics of a polymer model of a superhelical plasimd. We used a Brownian dynamics algorithm to calculate the time trajectory of the system. A subsequent simulation of the FCS process allows us to show the possible effect of the rotational dynamics of the attached fluorophore on the experimental outcome.
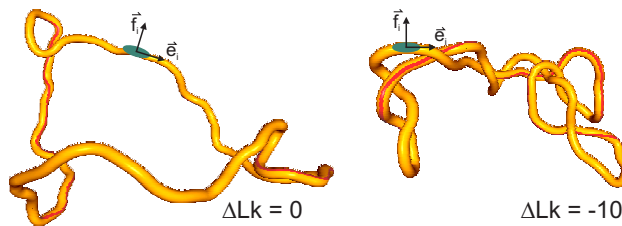

Figure 1: The figure shows two representative conformations of superhelical DNA for $\Delta Lk = 0$ and $\Delta Lk = -10$. The attached fluorophor is shown in green together with its two local direction vectors $\vec{e}_i$ and $\vec{f}_i$.

2 Theory and Methods

2.1 Brownian dynamics algorithm

We use a Brownian dynamics (BD) algorithm that is described in detail in Ref.[17,18] Here we present only the basic principles of the simulation. The DNA is modeled as a chain of N linear segments with $N+1$ beads assigned at each joint $\vec{r}_i$. To each segment a system of three orthogonal vectors of unit length is attached $(\vec{f}_i, \vec{e}_i, \vec{g}_i)$, where $\vec{e}_i$ points into the direction of the ith segment. In a closed circular chain, bead $N+1$ coincides with the first bead. The energy of the system is given by harmonic potentials for

the bending angles between adjacent segments, the twisting angles between assigned orientations of adjacent segments and deviations from the equilibrium segment length. The electrostatic interaction between different non-adjacent segments is calculated using a Debye-Hückel potential with a renormalized linear charge density of DNA as described by Ref.[19] The simulations were performed using a second-order Brownian dynamics algorithm. Hydrodynamic interactions between the beads are described by the Rotne-Prager tensor[20] for translation diffusion, while rotation around the segment axis is given by the rotational diffusion coefficient D_{rot}. The model allows for permanently bent sequences, deviating from the average colinearity of adjacent segments vectors $\vec{e}_i$ and $\vec{e}_{i-1}$ at thermal equilibrium in the case of non-bent sequences. An auxiliary unit vector $\vec{b}_i$ with the polar coordinates $(\phi^\star, \theta^\star)$ in the local coordinate system is introduced at the bent ith joint, such that the relevant bending angle for the bending energy is now calculated between $\vec{e}_{i-i}$ and $\vec{b}_i$.

2.2   Monte Carlo algorithm

A starting conformation for the Brownian dynamics simulation is generated by a Monte Carlo (MC) procedure. The Monte Carlo algorithm is derived from Ref.[21] and uses the modifications implemented in Ref.[22] The definition of the segments and beads is identical to the Brownian dynamics simulation. The energy terms have also been adopted, except that no deviations of the equilibrium segment length l_0 are allowed. The Monte Carlo algorithm uses two different Monte Carlo steps. 1. In a pivoting step, a subchain of 2-10 segments is randomly chosen, and rotated about its end-to-end vector by the angle β uniformly distributed in an interval $(-\beta_0, \beta_0)$. The fraction of this pivoting step is 2/3, and the overall acceptance rate is $\approx 50\%$.
2. In a reptation step a randomly chosen subchain of 5 segments is exchanged with a randomly chosen subchain of 4 segments, if the end-to-end distance of the 5-segment subchain is not longer than 4 segments. Each subchain was deformed by changing the end-to-end distance such that it could be incorporated at the position of the other subchain. The deformation of a subchain was realized as a sequence of rotations of the individual segment vectors $\vec{s}_i$ until the condition for the end-to-end distance was

fulfilled. Here each subchain segment was rotated around the vector $\vec{s}_i \times \vec{X}$ by a small angle proportional to $|\vec{s}_i \times \vec{X}|$, where $\vec{X}$ is the subchain end-to-end vector. The orientation of the inserted subchain was chosen such that the orientation of the center-of-mass with respect to the end-to-end axis coincides with the orientation of the center-of-mass of the exchanged subchain. The fraction of the reptation step is 1/3.

The acceptance of the MC pivoting step is the same as in the standard Metropolis algorithm. Regarding the reptational step the modifications of Ref.,[22] which take into account the entropy change by adjusting the end-to-end distance of the subchains, have been kept the same. From the initial conformation 10^8 Monte Carlo steps have been calculated to obtain the starting conformation for the Brownian dynamics simulation.

2.3   Model of superhelical and linear DNA

As a model system for studying the dynamics of superhelical DNA we use the pUC18 plasmid. The pUC18 plasmid contains 2686 basepairs, therefore we approximate the circular DNA by a closed chain of $N = 91$ linear segments of length $l_0 = 10$ nm. The bending persistence length l_p of the simulated DNA is set to 50 nm. The experimentally determined values for the torsional elastic constant range from 2.0×10^{-19} erg cm,[23] 2.2×10^{-19} erg cm[24] to $\approx 3.0 \times 10^{-19}$ erg cm.[25,26] For the simulations we adopt an intermediate value of $C = 2.5 \times 10^{-19}$ erg cm. The DNA stretch modulus was set to 63.3 pN, softer than the experimental value.[27] As it was shown in Ref.,[28] a softer elastic stretch modulus does not alter significantly statistical properties such as end-to-end distances and corresponding relaxation times, while it allowed to lower computation time. The bead radius is adjusted such that the translational diffusion coefficient of n beads placed equidistantly in a row with a distance l_0 equals the translational diffusion coefficent of a cylinder with hydrodynamic radius r_{HD} and length nl_0. The diffusion coefficient of a cylinder can be calculated as described in Ref.,[29,30] while the diffusion coefficient for the string of beads is given in the work of Hagerman et al.[31] For the hydrodynamic radius r_{HD} of DNA we set the value to 1.2 nm according to Ref.[31] The rotational diffusion coefficient equals a cylinder with radius r_{HD}: $D_{rot} = k_B T / 4\pi\eta r_{HD}^2 l_0$. We studied the circular DNA at different superhelical densities $\sigma = \Delta Lk / Lk_0$ e.g. from

6

an relaxed DNA at $\sigma = 0$ ($\Delta Lk = 0$) to $\sigma \approx -0.015$ ($\Delta Lk = -4$) and $\sigma \approx -0.037$ ($\Delta Lk = -10$). For the linear DNA the same elasticity parameters and contour length were used as for the circular DNA. All simulations were done at 0.1 M salt conditions and a temperature $T = 293.15$ K. The time step was set to $\Delta t = 1$ ns. Table 1 summarizes all used simulation parameters.

Parameter	Description	Value
Δt	simulation time step	1.0 ns
T	temperature	293.15 K
I	ionic strength	100 mM
η	viscosity	10^{-3} Pa s
D	dielectric constant	80.18
N	number of segments	91
l_0	equilibrium segment length	10 nm
δ	elastic stretch modulus	63.3 pN
B	Kuhn length	100 nm
C	torsional rigidity constant	2.5×10^{-19} erg cm
r_{HD}	hydrodynamic DNA radius	1.2 nm

Table 1: BD and MC simulation parameter values

2.4 FCS simulation:

In order to model the outcome of FCS measurements on the simulated DNA, we have developed a program that uses the BD trajectories to calculate the expected fluorescence intensity $I(t)$ for a labeled DNA diffusing through the focus of a FCS setup. The normalized autocorrelation curve $g(\tau) = \langle I(t+\tau) \cdot I(t) \rangle / \langle I \rangle^2$ was calculated by use of a multi-τ correlation algorithm.[32,33] Here $\langle \rangle$ denotes temporal averaging over time t. This algorithm is also used by hardware correlator cards widely employed in FCS experiments. Each trajectory is a time series of the spatial positions of a single bead $\vec{r}_i(t)$ to which the fluorophore is attached. It may also contain the orientations $\hat{p}_i(t)$ ($|\hat{p}_i(t)| = 1$) of the fluorophore's dipole vector, which can be represented as a superposition of the segment vectors $\vec{e}_i$ and $\vec{f}_i$ in the local reference frame. The dipole

vector accounts for the interaction of (partially) polarized excitation light with the fluorophore. If a fraction $F_{pol} \in [0,1]$ of the excitation light is linearly polarized, parallel to a unit vector $\hat{\varepsilon}_{ex} = (1,0,0)$, then according to Ref.[34] the excitation probability is reduced:

$$f_{pol}(\hat{p}_i(t)) = (1 - F_{pol}) + F_{pol} \cdot (\langle \hat{\varepsilon}_{ex}, \hat{p}_i(t) \rangle)^2 \leq 1, \tag{1}$$

where $\langle \cdot, \cdot \rangle$ denotes the Euclidean scalar product. The number of detected photons $N_{phot}(t) \propto I(t)$ is calculated by first estimating the average number $\overline{N}_{phot}(t)$ of photons expected in one simulation step $[t, t + \Delta t_{FCS}]$. Then $N_{phot}(t)$ is drawn from a poissonian distribution with average $\overline{N}_{phot}(t)$. This procedure accounts for the counting statistics of the photon detection. The expected photon number is given as

$$\overline{N}_{phot}(t) = \overline{N}_0 \cdot \Delta t_{FCS} \cdot \sum_{i=1}^{K} q_f \cdot q_{det} \cdot h(\vec{r}_i)^2 \cdot f_{pol}(\hat{p}_i(t)). \tag{2}$$

Here K denotes the number of fluorophores near the laser focus, $\overline{N}_0$ is the maximum number of possibly detected photons per fluorophore and time step, while q_f and q_{det} are the quantum efficiencies of fluorescence and detection, respectively. The form of the excitation and detection profile, which are assumed to be identical and completely overlapping, is described by

$$h(x,y,z) = \exp\left(-2 \cdot \frac{x^2 + y^2}{w_{xy}^2} - 2 \cdot \frac{z^2}{\gamma^2 w_{xy}^2}\right). \tag{3}$$

The lateral width of the profile is w_{xy} and $\gamma = w_z / w_{xy}$ is its aspect ratio, where w_z is the focal width in z direction.

Note that we neglect photophysical dynamics in the system, such as bleaching or triplet blinking, as we want to observe the effects of the DNA motion only. The photophysics could be introduced into the simulation by making the fluorescence efficiency q_f time dependent and changing it for every particle with a suitable simulation. A full simulation, but without the effects of polarization has been described in Ref.[35] In real experiments care has to be taken to discriminate inevitable photophysical effects from the other contributions to the measured correlation function. The typical timescale of

the triplet dynamics is $[0.1\mu s, 10\mu s]$,[14] which is near the expected effect of the rotational dynamics.

For the simulations the trajectories were shifted in time and space so that they pass the focus consecutively. Each trajectory of length M was shifted to satisfy $\vec{r}_i(M/2) \equiv 0$. This ensures that in average there is less than one particle in the focus which mimics real experiments in strongly diluted solutions. In order to still obtain reasonable photon statistics from only few trajectories that were simulated, we raised the fluorescence efficiency to an unrealistically high value of $q_f = 10$. We compared simulations for $q_f < 1$ and $q_f = 10$ and found that this change improves the statistics but does not change the results in any other respect. Refer to Table 2 for an overview of the FCS simulation parameters used to generate the data.

Parameter	Description	DNA	test system
Δt_{FCS}	FCS simulation time step	$1\ \mu s$	$1\ \mu s$
Δt_{br}	Brownian motion time step	—	$0.2\ \mu s$
$T_{trajectory}$	length of a single trajectory	0.5 s	—
T_{sim}	length of diffusion simulation	—	50 s
$\overline{N}_0$	absorbed photons per molecule	$\approx 6 \cdot 10^6\ s^{-1}$	$10^7\ s^{-1}$
w_{xy}	lateral width of excitation profile	$0.5\ \mu m$	$0.5\ \mu m$
q_f	fluorescence quantum yield	10	0.97
q_{det}	detection efficiency	0.1	0.1
$\hat{\varepsilon}$	excitation light polarization	$(1,0,0)$	$(1,0,0)$
c	concentration of simulated particles	—	$0.3\ \mu m^{-3}$

Table 2: FCS simulation parameter values for the DNA simulations and the diffusion simulations of the test system.

2.5   Test Diffusion Simulation

As a test system for the FCS simulation we also used a simple Brownian motion simulation which calculates the trajectories of fluorophores inside a sphere around the laser focus. The size of the simulation volume was chosen to be at least five times larger than the laser focus width in each direction. The position $\vec{r}_i(t)$ of the ith fluorophore

is updated in each simulation step Δt_{br} by a random vector $\Delta \vec{r}$, where each component is drawn from a gaussian distribution with zero mean and width $\sqrt{2D_{\mathrm{t}}\Delta t_{\mathrm{br}}}$. D_{t} denotes the given translational diffusion coefficient. If a particle leaves the simulation volume it is deleted from the simulation and a new particle is positioned at a random spot on the boundary of the volume such that the particle concentration remains constant. In addition this simulation also incorporates the rotational diffusion of the fluorophore's dipole vector $\hat{p}_i(t)$. In every time step, $\hat{p}_i(t)$ is updated with a random vector $\Delta \vec{p}$ while ensuring that $\langle \hat{p}_i(t), \hat{p}_i(t) + \Delta \vec{p}\rangle = \cos(\Delta \phi)$ and that $|\hat{p}_i(t) + \Delta \vec{p}| = 1$. Here $\Delta \phi$ is drawn from a gaussian distribution with width $\sqrt{2D_{\mathrm{r}}\Delta t_{\mathrm{br}}}$, where D_{r} is the given rotational diffusion coefficient. This results in a Brownian translational motion of the particle and an independent random walk of the tip of $\hat{p}_i(t)$ on a unit sphere. Table 2 summarizes the used simulation parameters.

3 Results

3.1 Homogeneous DNA

The Brownian dynamics simulation was used to calculate time trajectories of superhelical DNA with linking numbers $\Delta Lk = 0$ and -10. In the first set of simulations, the equilibrium bending angle between segments was set to 0, i.e., the chain had a straight equilibrium conformation. The polymer conformations described by the bead positions $\{\vec{r}_i\}$ and the segmental orientation $\{\vec{f}_i\}$ were recorded at a set of M discrete time points $\{t\}$. For long time trajectories, positions and conformations were saved every 1000th time step Δt. In order to resolve dynamics on shorter time scales, additional short time trajectories have been used, where conformations were recorded at every time step. For each set of parameters five long and five short time trajectories have been calculated with a length of 500ms and 100μs respectively. The short time trajectories allowed us to obtain properties like the mean-square displacement (MSD) of a labeled bead in the time interval $[1\mathrm{ns}, 1\mu\mathrm{s}]$, while the longer time trajectories were used in the time range from 1μs to 50ms. All calculated properties were averaged over the simulated trajectories.

10

As a first step the translational diffusion coefficient D_t can be estimated from the slope of the center-of-mass trajectory. The center-of-mass $\vec{r}_{cm}$ is defined as the average of the bead positions $\vec{r}_{cm} = (1/N)\sum_{i=1}^{N}\vec{r}_i$. The mean square displacement (MSD) of the center-of-mass displays strictly normal diffusion on all time scales. If we fit it according to the normal diffusion equation $\langle r_{cm}^2(\tau)\rangle = 6D_t\tau$ we obtain the translational diffusion coefficients $D_t = 3.9\,\mu m^2\,s^{-1}$ ($\Delta Lk = 0$) and $D_t = 5.0\,\mu m^2\,s^{-1}$ ($\Delta Lk = -10$). This reproduces the data found in dynamical light scattering experiments and MC simulations.[4] The shift to higher translational diffusion coefficients can be explained by the formation of a plectonemic, interwound structure at increasing linking number differences, which is more compact as seen in Figure 1. The internal motion of a bead $\langle \vec{r}_{rel}^2(\tau)\rangle$ relative to the center-of-mass is defined as

$$\langle \vec{r}_{rel}(\tau)^2\rangle = \frac{1}{M}\sum_{\{t\}}[(\vec{r}_i(t+\tau) - \vec{r}_{cm}(t+\tau)) - (\vec{r}_i(t) - \vec{r}_{cm}(t))]^2. \tag{4}$$

The simulated data for the internal motion of the labeled bead together with the overall MSD are depicted in Figure 2. At small time scales the internal motion follows a power law $\langle \vec{r}_{rel}^2(\tau)\rangle \propto \tau^\alpha$. For different linking number differences ΔLk we found the exponents $\alpha \approx 0.74$ ($\Delta Lk = 0$) and $\alpha \approx 0.72$ ($\Delta Lk = -10$), where we fitted in the time range $10^{-7}\,s < \tau < 10^{-5}\,s \ll \tilde{\tau}_1$. For comparsion we studied also linear DNA with the same contour length of 910 nm, where the labeled bead was positioned in the DNA center. The linear DNA yields an exponent $\alpha \approx 0.74$. The exponents are close to $3/4$, which is expected for the dynamics of linear semiflexible polymers at length scales below l_p.[36] At times longer than the longest relaxation time $\tilde{\tau}_1$ the internal motion saturates at a constant value. The longest relaxation time in the case of the linear polymer is $\tilde{\tau}_1 \approx 1$ ms as calculated from the autocorrelation of the end-to-end vector. At very short times $\tau < 10^{-8}$ s the exponent falls into the range between 0.8 and 0.9, which is due to the discretization of the BD model. In Figure 2 we included analytical calculations for the internal motion $\langle \vec{r}_{rel}^2(\tau)\rangle$ of a monomer in the center of a linear DNA, based on a Gaussian semiflexible chain as described in Ref.[37] and summarized shortly in the appendix.
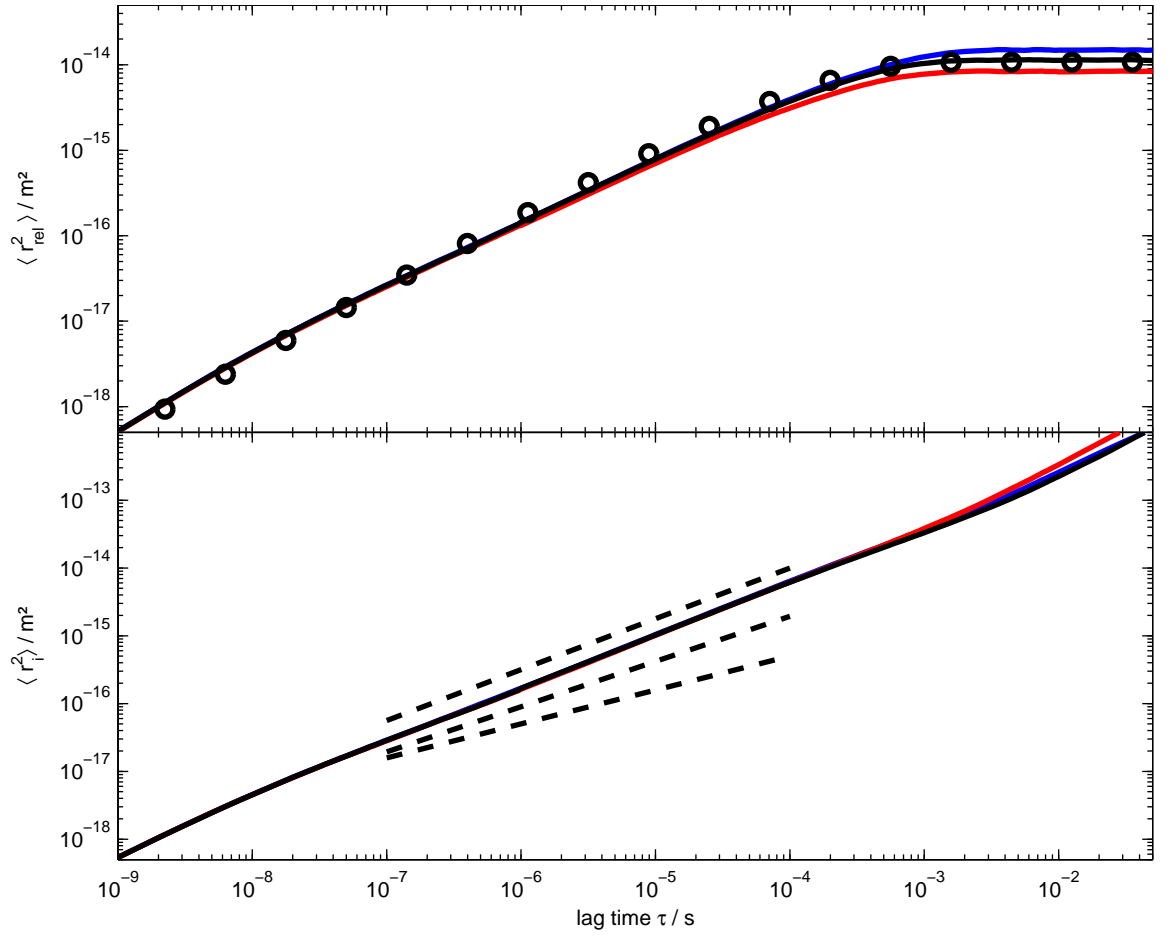
Figure 2: (a) The figure shows the MSD $\langle r_{rel}^2 \rangle$ of the DNA monomer relative to the center-of-mass for circular DNA with different linking number differences $\Delta Lk = 0$ (*blue*), $\Delta Lk = -10$ (*red*) and for a linear DNA (*black*). The symbols (*circles*) indicate the analytical prediction for a linear semiflexible polymer. (b) The total MSD $\langle r_i^2 \rangle$ was calculated showing the additional contributions of center-of-mass diffusion for the linking numbers $\Delta Lk = 0$ (*blue*), $\Delta Lk = -10$ (*red*) and linear DNA (*black*). The dashed lines mark a $\tau^{3/4}$-, $\tau^{2/3}$- and $\tau^{1/2}$-power law to guide the eye (*from top to bottom*).

The MSD of a labeled bead $\langle r_i^2 \rangle$ as a superposition of the internal dynamics and the center-of-mass motion, obeys at small times approximately the 3/4-power law of the internal motion. In this time range the differences between the $\Delta Lk = -10$ and $\Delta Lk = 0$ MSD curves do not exceed 4 % . For times $t \gg \tilde{\tau}_1$ the contribution from the internal motion becomes negligible and the dynamics are dominated by the center-of-mass

diffusion. We defined a local time-dependent exponent $\beta(\tau)$ by fitting a power-law $\langle \vec{r}_i^2(\tau) \rangle \propto \tau^\beta$ in the interval $[0.1\tau, 10\tau]$ around each τ. The results are shown in Figure 3. For the Rouse and Zimm model the MSD scales in the limit $\tau \ll \tilde{\tau}_1$ with a power law $\tau^{1/2}$ and $\tau^{2/3}$, respectively.[38] For linear end-labeled dsDNA fragments of different length L results consistent with the Zimm regime have been experimentally observed only for very long polymers exceeding $10^4 - 10^5$ bp[39] (and references therein), which corresponds to the limit of flexible polymers $L \gg l_p$. In Ref.[16] the Zimm regime was also observed for the longest measured linear dsDNA molecule of 23.1 kbp. However, for intermediate time scales an additional Rouse regime was reported for 2.4 to 23.1 kbp dsDNA. A recent theoretical study[40] showed also the existence of a sub-Zimm regime for end-monomer MSD, but could also not explain the observed Rouse regime. Interestingly, in a subsequent study[5] with superhelical pUC18 plasmids an exponent $\beta \approx 0.5$ typical of Rouse dynamics was found at intermediate times $\tau \approx 100\,\mu s$.

Here, our BD simulations based on a homogeneously elastic chain do not display an intermediate regime as reported in Ref.,[5] and which could have been attributed to Rouse- or Zimm-like dynamics; the local exponent β remains above 0.7 on all time scales. However, we do see a shallow minimum in the local exponent as proposed recently in Ref.,[40] reflecting the crossover from the stiff-rod limit to the flexible chain limit and then to normal translational diffusion. At higher superhelical densities this effect is diminished.
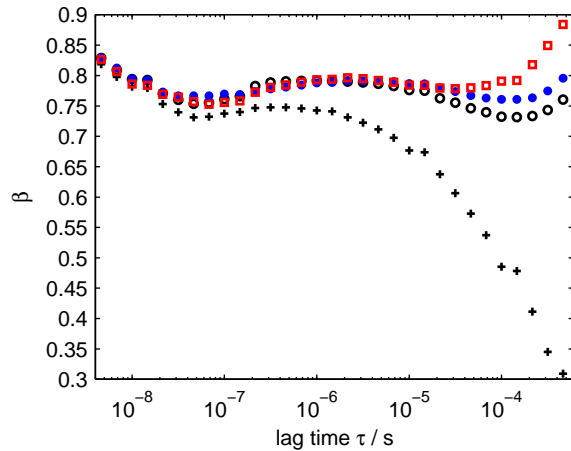
Figure 3: The time-dependent local exponent $\beta\,(\tau)$ of the MSD power-law $\langle r_i^2 \rangle \propto \tau^{\beta(\tau)}$ was obtained by fitting in the time interval $[0.1\tau, 10\tau]$. The local exponent is shown for the linear (*black circle*) and the circular DNA for a linking number difference $\Delta Lk = 0$ (*blue dot*) and $\Delta Lk = -10$ (*red square*). In addition the *crosses* indicate the local exponent $\alpha\,(\tau)$ for internal motion of linear DNA.

An important finding in[5] was a significant acceleration of the internal dynamics of DNA with increasing superhelical density. This can be compared to our earlier dynamic light scattering (DLS) experiments,[4] where the internal dynamics were quantitated by two parameters: the amplitude of internal motions and an internal diffusion coefficient, a measure of the motions of the smallest rigid DNA subunit in the superhelix. There the amplitude decreased nonmonotonically for increasing superhelical densities, displaying a local maximum at $\sigma \approx -0.03$, while the internal diffusion coefficient significantly increased for superhelical densities $|\sigma| \geq 0.04$.

In our current simulations as in,[5] the internal motion is measured as the relative displacement of the DNA monomer with respect to the center of mass of the molecule (Figure 2). For long times $\tau > \tilde{\tau}_1$ it approaches the constant value $2\langle a^2 \rangle$, where a signifies the amplitude of internal motion. We obtain the amplitudes $a = 86.1$ nm ($\Delta Lk = 0$) and $a = 65.5$ nm ($\Delta Lk = -10$). The decrease can be rationalized due to the more interwound, tighter structure for higher superhelical densities, which restricts the motion of the individual segments. However, in the simulations with homogeneously elastic, straight equilibrium DNA, the MSD of the internal motion (see Figure 2) displays no

14

acceleration of the dynamics for higher linking number differences.

3.2 Permantly bent sequences

As a possible explanation, it had been suggested in Ref.[5] that the experimentally observed acceleration of dynamics with increasing linking number difference might stem from a shift of the labeled segment towards the loop regions. pUC18 plasmid is known to contain permanently bent sequences.[3,41] The effect of the bent sequence is to organize the global structure by increasing the probability for an end loop at the bent sequence at high superhelical densities.[3] Therefore we simulated a circular DNA with a permanently bent sequence, which was introduced into the superhelices by assigning at three adjacent joints a bending angle $\theta^\star$ of 40° lying in the same bending plane ($\phi^\star = 0°$), such that the sequence spans a total bending angle of 120°. In one configuration of the system the labeled bead was placed directly at the bent sequence, such that the labeled bead remains a longer fraction of time in the end loops. In order to probe the dynamics in the stem region of the plectonemic structure, we also positioned the labeled bead at $\approx 25\%$ of the contour length L relative to the bent sequence. End loops were identified by using the method developed in Ref.[42] In analogy to the definition of the writhe Wr along the total contour,[38] this method defines a local writhe $\omega(j)$ in the vicinity of a segment j. The Gauss integral describes then the average number of cross-overs between the two tails of k segments ($k = 18$) at the segment j:

$$\omega(j) = \frac{1}{2} \int_{\vec{r}_{j-k}}^{\vec{r}_j} \int_{\vec{r}_{j+1}}^{\vec{r}_{j+k+1}} [d\vec{r}_1 \times d\vec{r}_2] \frac{\vec{r}_1 - \vec{r}_2}{|\vec{r}_1 - \vec{r}_2|}. \tag{5}$$

Segments which belong to the end loops in superhelices are characterized by high local writhe ω. We checked that the bend sequence correlates with a maximal average local writhe, while the second configuration showed on average a reduced local writhe.

As seen in Figure 4, positioning the fluorophore in the bent sequence greatly enhances its motion, especially for $\Delta Lk = -10$, which can be compared to the speed-up of end monomers relative to internal monomers in linear polymers, due to the on average greater fraction of time in an end loop. On the other hand the fluorophore dynamics are

diminished in the stem region at $\Delta Lk = -10$. For the more compact structure of higher superhelical densities the center-of-mass diffusion ($D_t = 4.9 \mu m^2\,s^{-1}$; $\Delta Lk = -10$) is faster than for the $\Delta Lk0$-structures ($D_t = 4.4 \mu m^2\,s^{-1}$; $\Delta Lk = 0$). Therefore the superposition of the internal and the center-of-mass motion for $\Delta Lk = -10$ cooperatively reinforces the acceleration at the bent sequence, resulting in a significant separation of the MSD curves in Figure 4. On the other hand, when the labeled bead is positioned at 25% of the contour length away from the bend, the difference between the MSD curves for $\Delta Lk = 0$ and $\Delta Lk = -10$ is diminished due to the opposing trends of the center-of-mass diffusion and the internal dynamics.
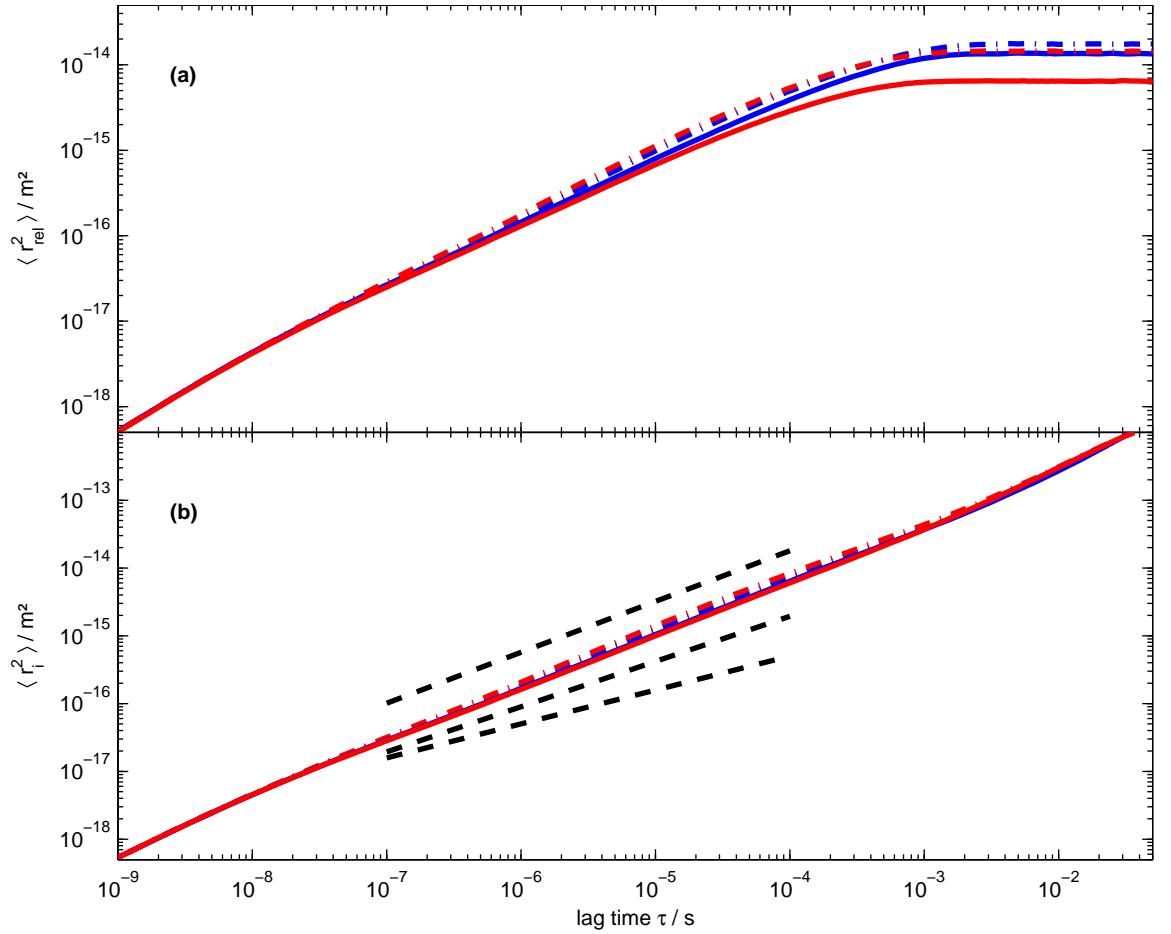
Figure 4: (a) The figure shows the MSD $\langle r_{\text{rel}}^2 \rangle$ of the DNA monomer relative to the center-of-mass for a superhelix with an intrinsically bent sequence for $\Delta Lk = 0$ (*blue*) and $\Delta Lk = -10$ (*red*) at the bend sequence (*dot-dashed*) and in a distance of $L/4$ relative to the bent sequence (*solid*). (b) The total MSD $\langle r_{\text{i}}^2 \rangle$ including the center-of-mass diffusion term is shown. The dashed lines mark a $\tau^{3/4}$-, $\tau^{2/3}$- and $\tau^{1/2}$-power law to guide the eye (*from top to bottom*).

As described in Methods, we simulated the FCS process from the trajectories obtained by the BD algorithm. Figure 5 shows the resulting normalized FCS correlation curves for superhelices which contain a bent sequence. A separation of the correlation curves with the linking number difference is visible if the monitored bead is at the bent sequence (see Figure 5(a)). Then higher linking number differences ΔLk imply faster decorrelation. In contrast we could not observe a splitting up any more, if the

labeled bead was shifted away from the bent sequence (see Figure 5(c)) or if the circular DNA did not contain a bent sequence (see Figure 8b). If the focus aspect ratio is increased to $\gamma = 5$, the splitting decreases, but the FCS correlation curves are still clearly distinguishable (data not shown).
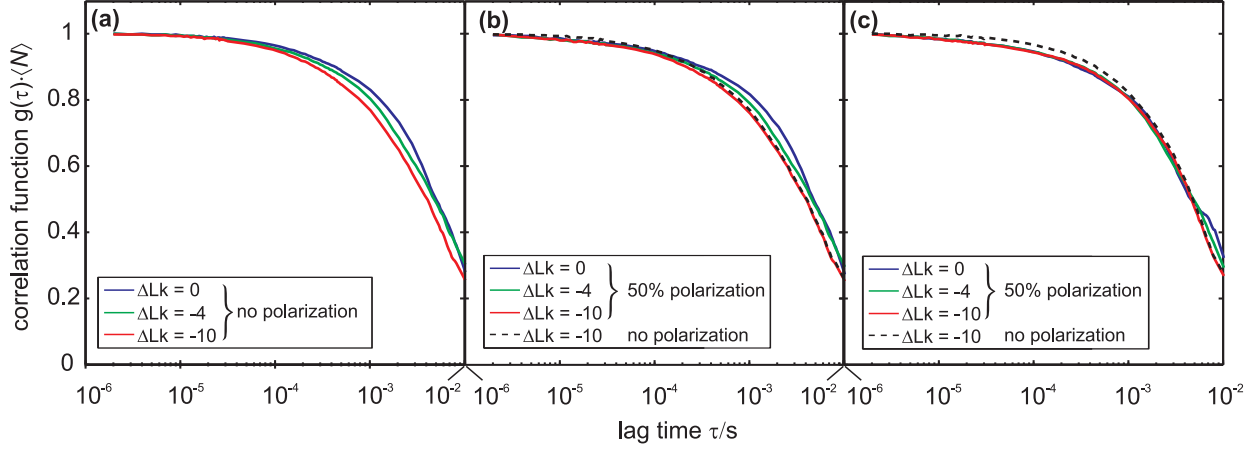

Figure 5: Normalized FCS correlation functions $g(\tau) \cdot \langle N \rangle$ of circular DNA at different linking number differences. For polarized light the dipole vector was set along the segment vector $\vec{e}_i$ and the focus axial ratio was $\gamma = 1$. (a) Fluorophore at the bent sequence and with unpolarized light, (b) fluorophore at the bend sequence and with 50% linearly polarized light and (c) fluorophore positioned at 25 % relative to the bent sequence and with 50% linearly polarized light.

3.3 Polarization

In the following we studied how the results are modified when polarization is included into the model of the FCS process. The dipole vector of the fluorophore is represented by a constant vector $\vec{p}_i$ in the local coordinate system $(\vec{f}_i, \vec{g}_i, \vec{e}_i)$ and can be expressed generally as a superposition of the $\vec{e}_i$- and $\vec{f}_i$-vector. Here we assume that the dipole vector is rigidly attached to one DNA segment and follows the translational and rotational motion of the segment. In experiments with superhelical DNA[5] a fluorophore is attached to the DNA by binding it to a third DNA strand that subsequently forms a triple helix. One end of the intercalating strand is then fixed to the ring. Under special experimental conditions this structure is known to be quite stable, which should make the fluorophore's dipole moment follow the ring dynamics. When the

triple helix is destabilized the fluorophore is connected to the superhelical DNA by a freely moving 10 nucleotide linker and thus the dipole moments direction should no longer correlate with the superhelical DNA conformation. The DNA is discretized with segments of equilibrium length l_0. Due to the discretization, normal modes of the semiflexible polymer which are associated with smaller length and time scales are not factored in. But modes of lenght scales smaller than $l_0 = 10$ nm are faster than the temporal resolution of a typical FCS setup and their contribution is therefore negligible. The rotating dipole moment is known to introduce an additional decay term into the FCS autocorrelation function, which is related to the dipole vector angular correlations $\langle \vec{p}_i(t+\tau)\vec{p}_i(t)\rangle$. From Figure 6 we can infer that the dynamics of the dipole vector at 25 % L from the bent sequence remains mostly unchanged compared to the linear DNA and to circular DNA without intrinsic bending. In contrast the superhelical $\Delta Lk = -10$-structure displays faster dynamics along the direction of the segment vector $\vec{e}_i = (\vec{r}_i - \vec{r}_{i-1})/|\vec{r}_i - \vec{r}_{i-1}|$. This is even enhanced if the fluorophore is attached directly to the bent sequence, which has an increased probability of being in an end loop. The dynamics perpendicular to the segment vector are clearly separated by two order of magnitudes from the dynamics parallel to the segment vector as shown in Figure 6(b), which simply reflects that twisting motions are faster than bending motions.[43] Only the decorrelation of $\vec{f}_i$ at the bent sequence is slowed down to time scales comparable to those of $\vec{e}_i$, which might indicate that the motions are not independent from each other. To extract the MSD $\langle \vec{r}_i^2(\tau)\rangle$ from the correlation curves, which have been normalized to satisfy $g(\Delta t_{\mathrm{FCS}}) = 1$, we applied the same approach as used for the experimental data published in Ref.,[5] and which is widely used for the analysis of FCS correlation functions. The transformation employed is described in the appendix. As seen in Figure 7 and Figure 8 a cross-over regime appears in between the stiff-rod limit and the normal translational diffusion. The slope of the intermediate regime depends on the fraction of linearly polarized light F_{pol}, but the appearance of this regime is independent of whether a bend has been inserted, and of the position of the observed bead. We only show exemplarily the results for $F_{\mathrm{pol}} = 0.5$ as this may be used to account for various experimental effects that disturb the polarization in the focus, or for imperfect

alignment of the fluorophore dipole. If for instance a non-polarization maintaining fiber is used in the setup or there are imperfections in a fiber, this may lead to temperature and strain dependent mixing of polarizations[44] (i.e. elliptical polarization at the output, which we model as superposition of non polarized and linearly polarized light). Also it is known that the polarization in the focus of an objective with high numerical aperture is elliptical if the objective is initially illuminated with linearly polarized light.[45]
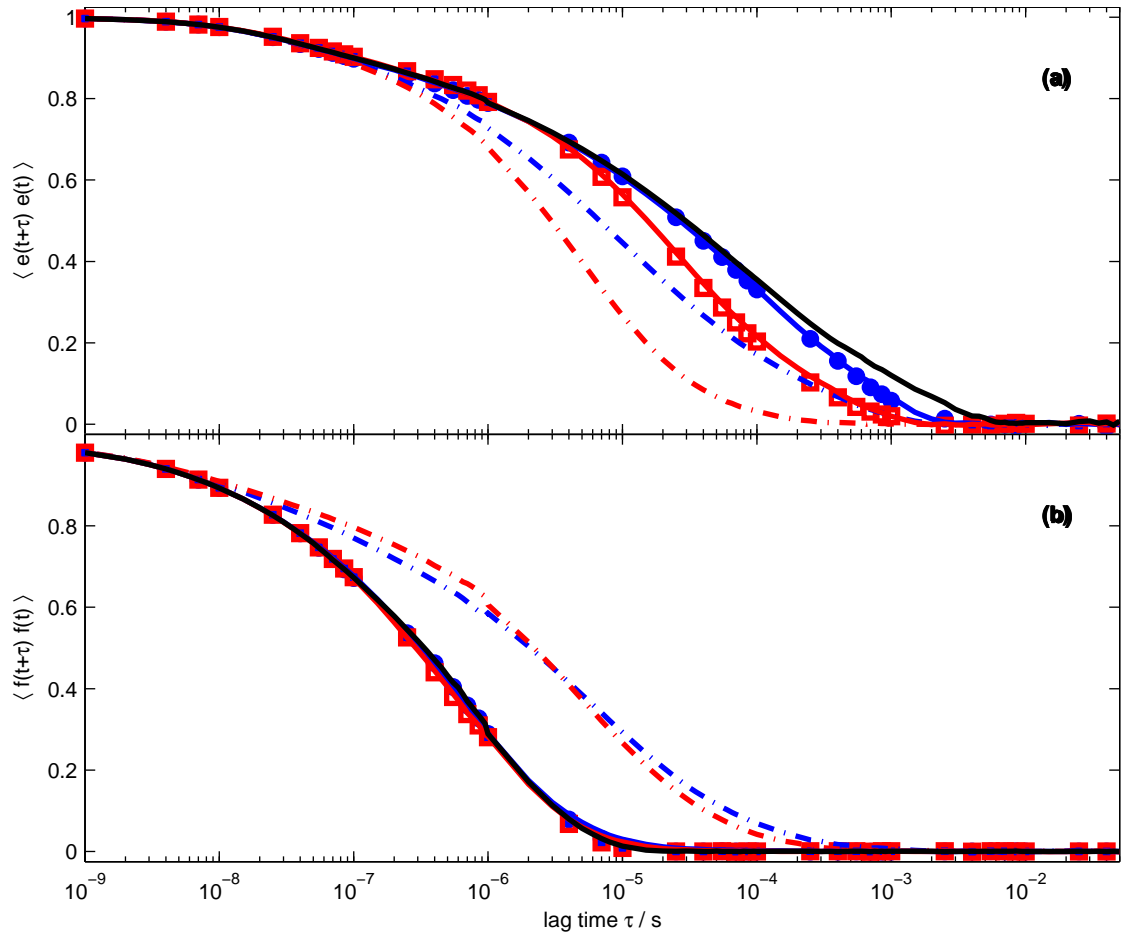
Figure 6: The figure shows the calculated temporal correlation of the dipole vector. The labeled bead was positioned directly at the bent sequence (*dot-dashed*), while in a second case a labeled bead in a distance of 25% of the total DNA contour length from the bend was introduced (*solid*) ($\Delta Lk = 0$ (*blue*); $\Delta Lk = -10$ (*red*)). DNA without permanently bent sequences is marked with *blue dots* ($\Delta Lk = 0$) and *red squares* ($\Delta Lk = -10$). For comparison the linear DNA is included (*solid black*). In (a) the dipole vector $\vec{p}_i$ has been aligned along the segment vector $\vec{e}_i$ and in (b) along the $\vec{f}_i$-vector.
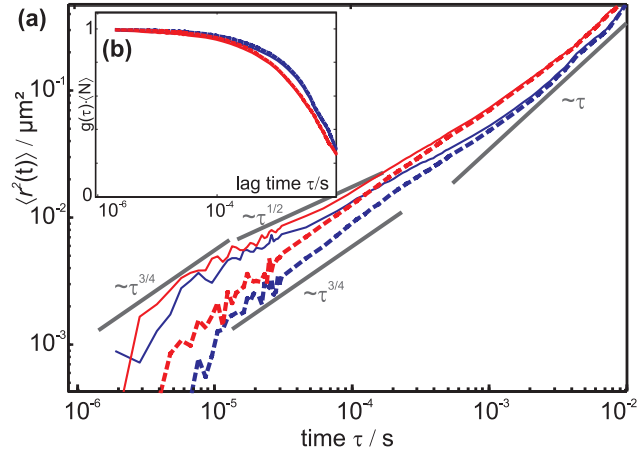
Figure 7: (a) MSD $\langle r_i^2(\tau) \rangle$ and (b) FCS correlation curves that were calculated for circular DNA with an intrinsic bend, where the labeled bead is positioned at the bent sequence. Results for two linking number differences $\Delta Lk = 0$ (*blue*) and $\Delta Lk = -10$ (*red*) are shown. Solid curves indicate 50% polarized excitation light and dashed curves show the results for unpolarized excitation.
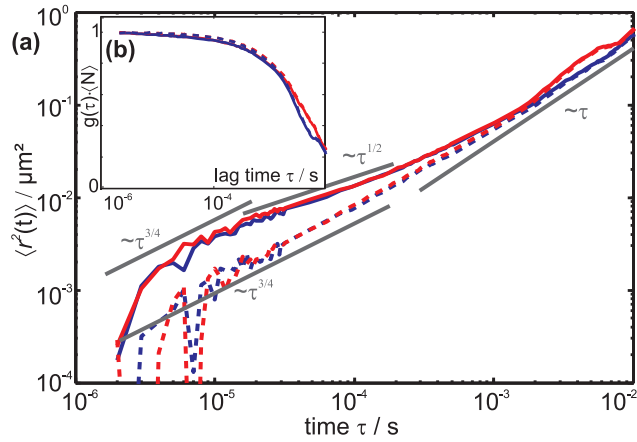

Figure 8: (a) MSD $\langle r_i^2(\tau) \rangle$ and (b) FCS correlation curves that were calculated for circular DNA without an intrinsic bend. Results for two linking number differences $\Delta Lk = 0$ (*blue*) and $\Delta Lk = -10$ (*red*) are shown. Solid curves indicate 50% polarized excitation light and dashed curves show the results for unpolarized excitation.

To further investigate the appearance of an intermediate regime we implemented a simple test system which consists of freely diffusing particles with rotationally diffusing dipole vectors. We simulated different runs which all had the same translational diffusion speed, while the rotational diffusion speed was changed. The correlation

22

times of both fractions were chosen to be in the same range as those from the DNA simulations. Figure 9(a) shows the resulting FCS autocorrelation functions which are normalized in a way that the translational diffusion parts overlap. This way one can directly observe the effect of the different rotation speeds on the correlation function. The rotational and diffusional motion are each characterized by a typical correlation time τ_r and τ_t. These times were extracted from the curves in Figure 9(a) by fitting them with a model, consisting of the standard factor for 3D normal diffusive motion and a factor for the rotational diffusion.[34] The model reads

$$
\begin{aligned}
g(\tau) \quad = \quad & \frac{1}{\langle N \rangle} \left[1 - F_{\text{rot}} + F_{\text{rot}} \left(c_1 \exp\left(-\frac{\tau}{\tau_r} \right) + c_2 \exp\left(-\frac{3\tau}{10\tau_r} \right) \right) \right] \cdot \\
& \cdot \left[1 + \frac{\tau}{\tau_t} \right]^{-1} \left[1 + \frac{\tau}{\gamma^2 \tau_t} \right]^{-\frac{1}{2}}
\end{aligned}
\tag{6}
$$

where F_{rot} represents the strength of the rotational part and $c_1 = 860/9, c_2 = 4$ were set to account for the setup of our virtual experiment, as described in Ref.[34] The results are incorporated in Figure 9(b), which shows the MSD curves extracted from the correlation curves that were normalized to $g(\Delta t_{\text{FCS}}) = 1$ as for the DNA simulations. We observe also an intermediate regime for excitation with partially polarized light, which can be attributed to the cross-over from rotational dynamics of the dipole vector to translation diffusion. The intermediate regime appears between the rotational and translational correlation times τ_r and τ_t, as long as the rotational motion can be resolved with the FCS setup or equivalently $\tau_r > \Delta t_{\text{FCS}}$. For $\tau_r \ll \Delta t_{\text{FCS}}$ the MSD curve approaches simply the curve for the normal translational diffusion. The results from this test system also confirm that the FCS simulation generates realistic correlation curves, as they have also been reported for comparable experiments (slowly rotating quantum dots) in Ref.[46] For the DNA simulations, where the fluorophore is excited with linearly polarized light, as shown in Figure 7 and Figure 8 the cross-over regime is therefore determined by the rotational dynamics of the fluorophore dipole vector (see Figure 6), the diffusion constant and the temporal resolution Δt_{FCS} of the FCS experiment.

A comparable interpretation[47] of results has been reported for single particle track-

ing measurements of fluorescence tagged phospholipid molecules in plasma membranes of living cells. The experimental data[48] show hop diffusion for this system with three clearly separated regimes in the RMS curve. Destainville *et al.*[47] explain these findings by a crossover between two regimes of normal diffusion characterized by different diffusion coefficients. On a fast timescale one observes the free normal diffusion of the phospholipids inside certain compartments of the membrane. On comparably longer timescales a slower normal diffusion is seen, that averages over the small timescales and describes the movement of the molecules between the compartments. These two regimes are interconnected by an anomalous intermediate regime similar to our findings for the test system and the superhelical DNA system.
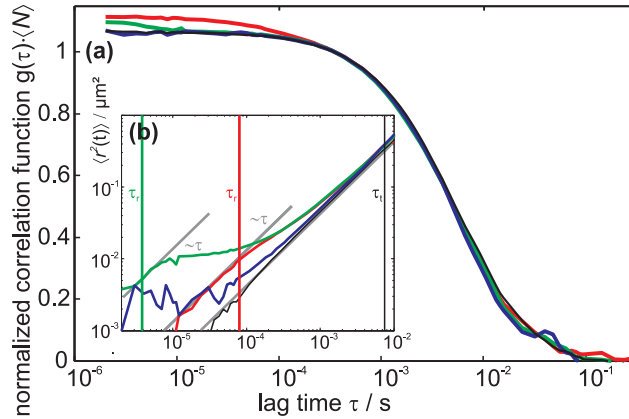

Figure 9: (a) shows the normalized FCS correlation function of the test system for non-polarized (black) and 50% linearly polarized excitation light (rotational diffusion coefficient increases in the order red — green – blue). The translational diffusion coefficient is $D_t = 4 \ \mu m^2 \ s^{-1}$ and $\gamma = 1$ for all curves. The FCS correlation curves have been normalized to $g(360 \ \mu s) = 1$. The inset (b) shows the MSD $\langle r_i^2 \rangle(\tau)$ we have extracted from the corresponding FCS correlation curves. The translational and rotational correlation times τ_t and τ_r, that were extracted using (6), are displayed (for the blue curve $\tau_r \ll \Delta t_{FCS}$). Note how they limit the intermediate regime.

4 Conclusions

In this work we studied the dynamics of circular DNA using a BD algorithm in which DNA is represented as a chain of linear segments.[17] Mechanical properties are included via harmonic potentials for bending, stretching and twisting of the segments

and electrostatics are treated within a Debye-Hückel approach. The BD generated time trajectories of the DNA conformations allowed us to simulate subsequently the FCS process of single labeled DNA and compare it to recent FCS experiments on superhelical DNA.[5] We focused on the question whether an acceleration of the dynamics with increasing superhelical density can be observed. Also we were interested whether an intermediate regime appears, which was reported in the experimental study, and there was associated with Rouse dynamics of the plasmid. The internal dynamics are governed by the physics of semiflexible polymers at short time scales. Inspecting the MSD at intermediate time scales showed a shallow minimum in the local exponent, which indicates the decrease of the internal motion before the onset of the normal translational diffusion as proposed in Ref.[40] Additionally this effect is even weakened for higher superhelical densities. Nevertheless for the studied DNA length of 910 nm the local exponent remains on all timescales well above $2/3$ for the Zimm and $1/2$ for the Rouse regime. For a homogeneously elastic, straight-equilibrium DNA chain we see no acceleration of the dynamics with increasing superhelical densities. Therefore we investigated how the insertion of permanently bent sequences into the DNA changes the dynamics. The positioning of the labeled DNA monomer with regard to the bent sequence strongly influences the motion due to the energetically favored formation of end loop-like structures at the bent site. The motion of beads near or in a bent sequence is enhanced while it is suppressed for beads that are positioned about 25% of the contour length away from the bent sequence. For higher superhelical densities this effect is more pronounced, which in turn with the more compact structure and higher translational diffusion coefficient results in an accelerated dynamics. Consequently the corresponding FCS autocorrelation curves differ dependent on the superhelical density. By taking fluorophore polarization explicitly into account, our FCS simulations can explain the experimentally observed apparent Rouse-like regime, under the assumption that the dipole is rigidly attached to the DNA segment. If the fluorophore is excited with partially polarized light we can show that an intermediate regime with a reduced local exponent appears in the FCS autocorrelation curves. These simulation results directly imply further experiments that could shed more light on the system at hand, by

25

testing and quantifying the polarization dependence of the FCS curves. The simplest possibility would be to compare measurements with linearly polarized and circularly polarized light as this can be implemented experimentally quite easily by introducing a $\lambda/4$ waveplate into the excitation laser beam path.

The contributions of polarized excitation are commonly not visible in FCS experiments, as the decorrelation time of the dipole vector is well below the fastest resolvable time scales. For the simulations presented here, the dipole vector dynamics are slow enough to become accessible in experiments. Thus we conclude that the intermediate regime originates from the visibility of two well separated decay terms for the translational and the rotational motion in the autocorrelation curve and polarization effects have to be taken into account in the analysis and interpretation of FCS data.

5   Appendix

5.1   Dynamics of Gaussian semiflexible chain

An analytical description of the dynamics of a Gaussian semiflexible chains has been given in the work of Harnau, Winkler and Reineker.[37] A polymer chain can be represented as a continuous, differentiable space curve $\vec{r}(s,t)$ with the contour coordinate $s \in [-L/2, L/2]$. The equation of motion of the Gaussian semiflexible polymer including hydrodynamic interactions is given by a Langevin equation, which can be solved by an expansion in terms of the eigenfunction $\psi_k(s)$. The internal motion is then given according to Eq. (4.3) by

$$\langle \vec{r}_{\mathrm{rel}}^2(t) \rangle = \frac{2k_{\mathrm{B}}T}{\pi\eta} \sum_{k=1}^{\infty} \tau_k \psi_k^2(s) \left(1 - \exp\left(-\frac{t}{\tilde{\tau}_k} \right) \right), \tag{7}$$

where τ_k are the relaxation times in the free draining limit (Eq. (2.29)) and the relaxation times $\tilde{\tau}_k$ (Eq. (3.10)) as denoted in Ref.[37] In order to compare the analytical solution with the simulation, we calculated the internal motion $\langle \vec{r}_{\mathrm{rel}}^2 \rangle$ for a chain of contour length L of 910 nm, a Stokes diameter of a bead $d = 2.4$ nm and at identical temperature T and viscosity η. A high-frequency cutoff of $\Lambda = 150$ was set for the

number of contributing modes in the sum in Eq.(7). The internal motion was evaluated at the DNA center $s = 0$.

5.2 Extracting $\langle \vec{r}_i^2(\tau) \rangle$ from correlation functions

FCS measurements produce correlation functions $g(\tau)$. These may be converted into the mean square distance function $\langle \vec{r}_i^2(\tau) \rangle$, which characterizes the Brownian motion of the fluorescing probes. As described in Ref.[5,39] the theoretical model for fluorescing particles in a gaussian focus reads:

$$g(\tau) = g_0 \cdot \left(1 + \frac{2}{3} \cdot \frac{\langle \vec{r}_i^2(\tau) \rangle}{w_{xy}^2}\right)^{-1} \cdot \left(1 + \frac{2}{3} \cdot \frac{\langle \vec{r}_i^2(\tau) \rangle}{\gamma^2 w_{xy}^2}\right)^{-1/2}, \qquad (8)$$

where g_0 is a normalization constant which we chose in accordance with Ref.[5,16] to be $g(\Delta t_{FCS})$. We then numerically inverted (8) to obtain $\langle \vec{r}^2(\tau) \rangle$. For the last step, we employed the `fsolve()` method from the Matlab 2008a numerics package with default parameters.

6   Acknowledgement

References

[1] J. White, *Am. J. of Mathematics*, 1969, **91**, 693–728.

[2] S. Wasserman and N. Cozzarelli, *Science*, 1986, **232**, 951–960.

[3] W. Kremer, K. Klenin, S. Diekmann and J. Langowski, *EMBO J.*, 1993, **12**, 4407–4412.

[4] J. Langowski, U. Kapp, K. Klenin and A. Vologodskii, *Biopolymers*, 1994, **34**, 639–646.

[5] R. Shusterman, T. Gavrinyov and O. Krichevsky, *Phys. Rev. Lett.*, 2008, **100**, 098102.

[6] E. Elson and D. Magde, *Biopolymers*, 1974, **13**, 1–27.

[7] E. Elson and D. Magde, *Biopolymers*, 1974, **13**, 29–61.

[8] M. Wachsmuth, W. Waldeck and J. Langowski, *JMB*, 2000, **298**, 677–689.

[9] M. Weiss, M. Elsner, F. Kartberg and T. Nilsson, *Biophys. J.*, 2004, **87**, 3518–3524.

[10] D. Magde, E. Elson and W. Webb, *Biopolymers*, 1978, **17**, 361–376.

[11] R. Koehler, P. Schwille, W. Webb and M. Hanson, *J. Cell. Sci.*, 2000, **113**, 3921–3930.

[12] P. Kask, P. Piksarv, . Mets and E. Lippmaa, *Eur. Biophys. J.*, 1987, **14**, 257–261.

[13] P. Kask, P. Piksarv, M. Pooga, U. Mets and E. Lippmaa, *Biophys. J.*, 1989, **55**, 213–220.

[14] J. Widengren, U. Mets and R. Rigler, *J. Phys. Chem.*, 1995, **99**, 13368–13379.

[15] D. Lumma, S. Keller, T. Vilgis and J. O. Rädler, *Phys. Rev. Lett.*, 2003, **90**, 218301.

[16] R. Shusterman, S. Alon, T. Gavrinyov and O. Krichevsky, *Phys. Rev. Lett.*, 2004, **92**, 048303.

[17] K. Klenin and J. Langowski, *Biophys. J.*, 1998, **74**, 780–788.

[18] T. Wocjan, K. Klenin and J. Langowski, *J. Phys. Chem. B*, 2009, **113**, 2639–2646.

[19] D. Stigter, *Biopolymers*, 1977, **16**, 1435–1448.

[20] J. Rotne and S. Prager, *J. Chem. Phys.*, 1969, **50**, 4831–4837.

[21] A. Vologodskii, S. Levene, K. Klenin, M. Frank-Kamenetskii and N. Cozzarelli, *J. Mol. Biol.*, 1992, **227**, 1224–1243.

[22] K. Klenin, M. Hammermann and J. Langowski, *Macromolecules*, 2000, **33**, 1459–1466.

[23] W. Taylor and P. Hagerman, *J. Mol. Biol.*, 1990, **212**, 363–376.

[24] P. Heath, J. Clendenning, B. Fujimoto and J. Schurr, *J. Mol. Biol.*, 1996, **260**, 718–730.

[25] D. Horowitz and J. Wang, *J. Mol. Biol.*, 1984, **173**, 75–91.

[26] D. Shore and R. Baldwin, *J. Mol. Biol.*, 1983, **170**, 983–1007.

[27] S. Smith and C. Bustamante, *Science*, 2006, **271**, 795–799.

[28] H. Jian, A. Vologodskii and T. Schlick, *J. Comp. Phys.*, 1997, **136**, 168–179.

[29] M. Tirado and J. de la Torre, *J. Chem. Phys.*, 1979, **71**, 2581–2587.

[30] M. Tirado and J. de la Torre, *J. Chem. Phys.*, 1980, **73**, 1986–1993.

[31] P. Hagerman and B. Zimm, *Biopolymers*, 1981, **20**, 1481–1502.

[32] K. Schatzel, *Inst. Phys. Conf. Ser.*, 1985, **77**, 175–84.

[33] D. Magatti and F. Ferri, *Appl. Opt.*, 2001, **40**, 4011–4021.

[34] S. R. Aragón and R. Pecora, *Biopolymers*, 1975, **14**, 119–138.

[35] J. Dix, E. Hom and A. Verkman, *J. Phys. Chem.*, 2006, **110**, 1896–1906.

[36] K. Kroy and E. Frey, *Phys. Rev. E*, 1996, **55**, 3092–3101.

[37] L. Harnau, R. Winkler and P. Reineker, *J. Chem. Phys.*, 1996, **104**, 6355–6368.

[38] M. Doi and S. Edwards, *The Theory of Polymer Dynamics*, Oxford University Press, Oxford, 1986.

[39] E. Petrov, T. Ohrt, R. Winkler and P. Schwille, *Phys. Rev. Lett.*, 2006, **97**, .

[40] M. Hinczewski, X. Schlagberger, M. Rubinstein, O. Krichevsky and R. Netz, *Macromolecules*, 2009, **42**, 860–875.

[41] G. Muzard, B. Théveny and B. Révet, *EMBO J.*, 1990, **9**, 1289–1298.

[42] K. Klenin, M. Frank-Kamenetskii and J. Langowski, *Biophys. J.*, 1995, **68**, 81–88.

[43] M. Barkley and B. Zimm, *J. Chem. Phys.*, 1979, **70**, 2991–3007.

[44] B. E. A. Saleh and M. C. Teich, *Funddamentals of Photonics*, John Wiley & Sons, 1991.

[45] B. Richards and E. Wolf, *Proc. R. Soc. London Ser. A*, 1959, **253**, 358–379.

[46] J. Tsay, S. Doose and S. Weiss, *J. Am. Chem. Soc.*, 2006, **128**, 1639–1647.

[47] N. Destainville, A. Sauliere and L. Salome, *Biophys. J.*, 2008, **95**, 3117–3119.

[48] K. Murase, T. Fujiwara, Y. Umemura, K. Suzuki, R. Iino, H. Yamashita, M. Saito, H. Murakoshi, K. Ritchie and A. Kusumi, *Biophys. J.*, 2004, **86**, 4075–4093.